

Decade-long Periodicity Study of 2FHL Blazars with Historical Optical Data

S. ADHIKARI¹,¹ P. PEÑIL¹,¹ A. DOMÍNGUEZ²,² M. AJELLO¹,¹ S. BUSON³,³ AND A. RICO¹

¹*Department of Physics and Astronomy, Clemson University, Kinard Lab of Physics, Clemson, SC 29634-0978, USA*

²*IPARCOS and Department of EMFTEL, Universidad Complutense de Madrid, E-28040 Madrid, Spain*

³*Julius-Maximilians-Universität, 97070, Würzburg, Germany*

Submitted to ApJ

ABSTRACT

In our recent investigation, we utilized a century's worth of archival optical data to search for a decade-long periodicity from the blazar PG 1553+113, finding a hint of a 22-year period. Building on this foundation, the current study extends our analysis to include 10 blazars from the Fermi Large Area Telescope 2FHL catalog to uncover similar long-term periodic behavior. To ensure the reliability of our findings, we consider the impact of observational limitations, such as temporal gaps and uneven sampling, which could potentially introduce artifacts or false periodic signals. Our analysis reveals that 4 of these blazars (AP Librae, MKN 421, MKN 501, PG 1246+586) exhibit decade-long periods in their optical light curves, albeit 3 of them may be influenced by noise. However, a likely genuine period of approximately 51 ± 9 yr is identified for MKN 421.

Keywords: BL Lacertae object, GLSP, WWZ, periodogram, methods: data analysis, time series analysis, gaps in timeseries

1. INTRODUCTION

Active galactic nuclei (AGN) are a phenomenon in the nuclei of galaxies that produce a tremendous amount of energy powered by the gas accretion onto a supermassive black hole compared to that of the aggregate of stars in the galaxy. If an accreting supermassive black hole (SMBH) launches its jet towards us from these nuclei, they are known as blazars (e.g., Peterson 1997; Wiita 2006).

Blazars show variability across the electromagnetic spectrum and at different timescales (Urry & Padovani 1995; Chakraborty et al. 2015; Acciari et al. 2011; Arbet-Engels et al. 2021). Traditionally, temporal variability in blazar light curves (LCs) is thought to range from intraday (\sim minutes - a day, Wagner & Witzel 1995) to long-term timescales (\sim months - years, Jurkevich et al. 1971). Recently, Peñil et al. (2020) identified years-long periodicity in γ -rays in some blazars. In addition to

that, recent studies using historical optical data on OJ 287 and PG 1553+113 hint towards even longer-term variability (Abdo et al. 2009; Dey et al. 2018; Peñil et al. 2024).

Decade-long variabilities in blazars provide valuable information on AGNs' physical processes and emission mechanisms (e.g., Bhatta 2021; Gupta et al. 2022; Peñil et al. 2024; Adhikari et al. 2024, A24 hereafter). The detection of decade-long quasi-periodic oscillations (QPOs) can favor certain emission mechanisms and scenarios, such as binary supermassive black hole (SMBH) systems or jet precession, which can significantly impact our understanding of the AGN central engine and its environment.

Binary SMBH systems are some of the models that explain long-term periodicity in blazars. In these systems, the interaction between two black holes can lead to periodic changes in the accretion rate and jet properties, resulting in observable QPOs (e.g., Tavani et al. 2018; Qian et al. 2019). The periodic gravitational influence of the secondary black hole on the accretion disk of the primary can cause variations in the emission intensity. For example, OJ 287 exhibits a \sim 12-year period

Corresponding author: Sagar Adhikari
E-mails: sagara@clemson.edu, ppenil@clemson.edu
majello@clemson.edu

associated with the binary orbit and a ~ 60 -year period due to the precession of the orbit (Dey et al. 2018). In addition, accreting binaries often hollow out a cavity and cause an overdensity in the circumbinary disk. The overdensity, referred to as a “lump,” can periodically modulate the accretion rate of the primary black hole, causing periodic modulation in the jet emission as explored for decade-long QPO of PG 1553+113 (A24).

Additionally, jet precession driven by the misalignment of the black hole’s spin axis and the accretion disk can produce QPOs (e.g., Rieger 2004). The precession causes the jet direction to change periodically, altering the observed emission when the jet orientation relative to our line of sight changes. This model is supported by multi-wavelength observations that show coordinated variability patterns over long timescales (e.g., Qian et al. 2018). Therefore, investigating decade-long QPOs in blazars not only provides an understanding of the dynamics of SMBH systems but also enhances a broader comprehension of jet physics and AGN variability, contributing to our knowledge of cosmic evolution and the role of AGN in shaping their host galaxies.

In A24, we analyzed historical optical LC of PG 1553+113 and found hints of ~ 22 yr periodicity along with a 2.2 yr period attributing the longer period to overdensity on the circumbinary disk. We also found that the period was unlikely to be an artifact of the sampling of data or gaps in the observations.

Based on A24, the present study expands our scope to investigate decade-long periodicity in the historical optical LCs of 203 blazars in the Second Catalog of Hard Sources (2FHL) published by the *Fermi*-Large Area Telescope (LAT) collaboration (Ackermann et al. 2016). This investigation also assesses the impact of data gaps on our periodicity analysis. By evaluating the potential for these gaps to create artifacts in the LCs, we mitigate the risk of misinterpreting observational gaps as genuine periodic signals, enhancing our findings’ robustness.

This work is organized as follows: §2 discusses access to historical optical data and data processing. §3 introduces the final sources for analysis using a general gap study on blazar-type data. The methodology is described in §4, followed by the results and discussion of the analysis and gap study in §5. Finally, the findings are concluded in §6.

2. DATA

We analyze optical data in our work primarily because optical telescopes have extensively monitored numerous blazars throughout the 20th century. In addition to

that, observations in other wavelengths do not offer the century-long observation required for our objectives.

We search for long-term oscillation in blazars starting from the 2FHL catalog, which helps us keep our initial sample size manageable. For these 203 blazars, we collect optical observations from various open-access databases.

2.1. Archival Optical Data

Digital Access to a Sky Century at Harvard (DASCH, Grindlay et al. 2009) provides public access to a historical optical archive of numerous blazars monitored throughout the 20th century. By scanning photographic plates collected over a century from telescopes worldwide, DASCH facilitates new studies in time-domain astronomy, particularly enabling investigations into searching for decade-scale periodicity in blazar emissions.

Given that the magnitude data was digitized from photographic plates, there are inherent quality issues with the scanned data points. To mitigate these issues, we utilize data points with no quality flags and errors less than ± 0.4 magnitude, as recommended¹.

2.2. Complementary databases

To complement the DASCH observations, we use data from other optical surveys, which provide V-band data on our sources of interest; Archives of Photographic PLates for Astronomical USE (APPLAUSE; Tuvikene et al. 2014)², The Katzman Automatic Imaging Telescope (KAIT; Filippenko et al. 2001)³, the Catalina Sky Survey (CSS; Drake et al. 2009)⁴, All-Sky Automated Survey for Supernovae (ASAS-SN; Shappee et al. 2014; Kochanek et al. 2017)⁵, American Association of Variable Star Observers (AAVSO)⁶ International Database, and Zwicky Transient Facility (ZTF; Masci et al. 2019)⁷. These databases extend the temporal coverage to 2024.

2.3. Data Processing

The photometry data from DASCH, AAVSO, ASAS-SN, CSS, ZTF, and ASAS-SN are compatible without needing any offset correction, so their LCs can be combined directly, as demonstrated by A24. A24 used constant magnitude sources, like V* W Vir, to verify the

¹ http://dasch.rc.fas.harvard.edu/database.php#AFLAGS_ext

² <https://www.plate-archive.org/applause/>

³ <https://w.astro.berkeley.edu/bait/kait.html>

⁴ <http://nessi.cacr.caltech.edu/DataRelease/>

⁵ <http://www.astronomy.ohio-state.edu/asasn/index.shtml>

⁶ <http://https://www.aavso.org/data-download/>

⁷ <https://www.ztf.caltech.edu/>

compatibility of different databases. We also found that V* W Vir’s magnitude is in calibration with the AP-PLAUSE database. Therefore, we can combine LCs from these databases without any adjustments.

3. SOURCE SELECTION

We obtained data for 11 of the 203 blazars included in the 2FHL *Fermi*-LAT catalog by searching the DASCH database. Excluding PG 1553+113 as it was examined in our earlier work (see A24), we combine the DASCH data with that from the complementary databases for our sources of interest, which are listed in Table 1 with their respective 2FHL source names, Right ascension (RA) and Declination (Dec) coordinates, and redshifts (Ackermann et al. 2016).

We analyze the observed data in 28-day intervals. This binning period allows us to focus on variations that extend beyond the short-term, intra-day, or week-long fluctuations typically observed in blazars. By adopting this approach, we can better identify the longer-term patterns for assessing decadal-scale periodicity in blazar emissions. The binned LCs of the tabulated sources after filtering outliers using Tukey’s fence method (Tukey et al. 1977) are shown in Appendix A1.

3.1. General Gap Study

Noticing the non-uniform sampling and gaps in the aforementioned LCs, we explore the impact of non-uniform sampling and gaps on periodicity study to further constrain the sample sources for our analysis. For that purpose, we simulate $N_{\text{sim}} = 10^6$ red-noise LCs with the power-law slope (α) 1.5 and amplitude (A) 0.45, serving as toy model estimations for blazar power spectral density (PSD). 28-day binned data points going from 1900 to 2024 are generated for each simulated LC. This artificial data represents ideal and regular sampling. To mimic uneven sampling, 40% of data is randomly removed, and to introduce regularly occurring gaps in the observations, an additional 45% of data is removed in three regular intervals. Errors for each data point on each LC are introduced from a normal distribution $\mathcal{N}(0, 0.2)$. This process results in LCs that are randomly sampled, featuring three regular gaps and sampling, similar to the real ones, of 15%. We then do a GLSP analysis on those LCs and calculate the significance of the highest peak in each of them against a red-noise signal. The result of this is shown in Figure 1. The density plot reported in the top panel shows the distribution of observed periods, corresponding to uniformly distributed peak frequencies along with some edge effects and we do not notice a preference for any particular period due to the gaps. The histogram on the right

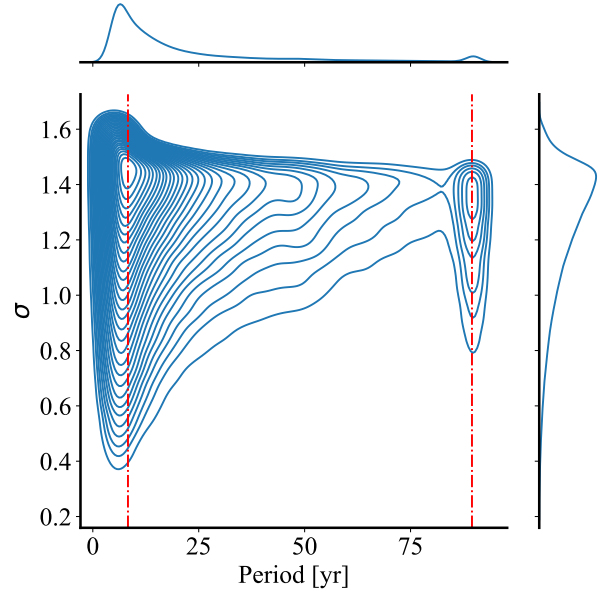


Figure 1. Distribution of observed peak periods and significances in the periodogram of simulated red-noise LCs with 85% data removed. The top histogram is similar to a uniform distribution of frequencies except for the edge effects. We see this edge effect as an enhancement in the 8.3 and 89.5 yr periods, represented by the red dotted lines.

shows the distribution of significances observed for peak periods in each LC; here, we notice a skewed Gaussian distribution with a mean significance of $\sigma_{\text{mean}} = 1.43$. The lopsided distribution hints at an increase in calculated significance due to gaps.

Additionally, we repeat the study for different fractions of sampling (such as 10%, 20%, and 25%) and find that for a sampling of $\geq 15\%$, there is no preference for false periodicity, but a decrease in their significance with increased sampling is noticed. Therefore, we select the sources with at least 15% sampling for our analysis.

3.2. Final Sample Sources

Finally, we select candidates for a periodicity study from the sources meeting the criterion defined in § 3.1. The final selected sources are AP Librae (with 15.4% sampling), M 87 (45.7%), MKN 180 (15%), MKN 421 (18.1%), MKN 501 (23.3%), and PG 1246+586 (15.9%).

The LCs of the sources selected and discarded from further analysis using this criterion are shown in Appendix A1.

4. METHODOLOGY

This section discusses the methodology we use for the QPO analysis and significance estimation.

4.1. Periodicity Estimation

Association Name	2FHL Source Name	RA (J2000)	Dec (J2000)	Redshift (z)
PKS 0754+100	J0756.8+0955	07 56 50.9	+09 55 12	0.266
TXS 1055+567	J1058.5+5625	10 58 35.0	+56 25 34	0.143
MKN 421	J1104.4+3812	11 04 28.8	+38 12 26	0.031
MKN 180	J1136.5+7009	11 36 34.1	+70 09 43	0.045
M 87	J1230.8+1225	12 30 49.0	+12 25 54	0.00428
PG 1246+586	J1248.1+5820	12 48 11.3	+58 20 24	–
PKS 1424+240	J1427.0+2348	14 27 01.9	+23 48 10	0.6035
PKS 1440–389	J1443.9–3909	14 43 59.3	–39 09 45	0.0654
AP Librae	J1517.7–2421	15 17 43.0	–24 21 16	0.048
MKN 501	J1653.9+3945	16 53 54.2	+39 45 14	0.0337

Table 1. Periodicity and trend study candidates with their 2FHL names, RA and Dec coordinates and redshifts.

The LCs of selected blazars are non-uniformly sampled, requiring periodicity estimation techniques that consider such time series data.

Generalized Lomb-Scargle Periodogram (GLSP, [VanderPlas 2018](#)) analysis and Weighted Wavelet Z-transform (WWZ, [Foster 1996](#)) are best suited to evaluate periodicity in such LCs, and both are widely used periodicity search methods in astronomy. In both methods, we search for periods in the range of 5 to 70 years following A24 for all blazars in our final sample.

4.1.1. Generalized Lomb-Scargle Periodogram

GLSP relates to the Fourier transform methods of periodicity analysis and the statistical method of least squares, so it has a unique position for the periodicity study of unevenly sampled time-series data ([VanderPlas 2018](#)). Fourier transform tells the relative amplitude of the frequencies present in the data, and the least square method of periodicity analysis is flexible for unevenly sampled time series data. Following A24, we use the [Astropy Collaboration et al. \(2022\)](#) implementation of GLSP on our dataset.

4.1.2. Weighted Wavelet Z-transform

WWZ is a robust method employed to discern periodic signals within blazar LCs in A24. By employing a Morlet wavelet, WWZ allows for a time-frequency decomposition of the LC, revealing regions of significant power corresponding to periodic features. This method incorporates weights into the wavelet transform, which enhances sensitivity to specific frequency bands and time intervals and facilitates the detection of periodic signals amidst noise and variability. WWZ is famously useful for data having irregular sampling and noise contamination. This method identifies periodic signals with varying strengths and durations (e.g., [Foster 1996](#)). It is also important to consider the edge effects in the wavelet analysis, often represented by the cone of influence (COI) in WWZ plots. This is a region in the WWZ

scalogram where the edge effects become significant, and the presence of a particular frequency becomes less reliable due to the decrease in the number of data points in the Morlet wavelet. In this work, we use the WWZ implementation of [Khider et al. \(2020, PYLEOCLIM\)](#)⁸.

4.2. Significance levels

Periodicity searches face challenges due to noise, which appears as erratic brightness fluctuations termed red noise ([Papadakis & Lawrence 1993; Vaughan et al. 2003; Zhu & Xue 2016](#)). We assess the significance of periods present in time-series data for a complete periodicity analysis.

For that purpose, we simulate 10^6 artificial LCs to determine the significance of detected periods and estimate the likelihood of false positives. These artificial LCs, generated following the technique of [Emmanoulopoulos et al. \(2013\)](#) using the Python implementation by [Foreman-Mackey et al. \(2013\)](#), possess the same PSD, probability density function, and sampling characteristics as the real LCs. We consider two PSD models, power law (PL) and bending power law (BPL), to generate artificial LCs; the former provides a general prescription of red noise, and the latter provides a more realistic model of blazars' variability across all timescales (e.g., [Chakraborty & Rieger 2020](#)). Subsequently, we analyze the resulting periodograms to determine the confidence levels of their peaks, calculated based on percentiles of the power for each period bin in the periodograms.

4.3. Power spectral density estimation

Traditionally, noise is categorized based on the power-law index α of the PSD equation $A * \nu^{-\alpha}$, where ν represents frequency (yr^{-1}), and A denotes normalization ([Rieger 2019](#)). Additionally, for the BPL, we utilize the

⁸ https://github.com/LinkedEarth/Pyleoclim_util

formula from Chakraborty & Rieger (2020):

$$P(\nu) = A \left(1 + \left\{ \frac{\nu}{\nu_b} \right\}^\alpha \right)^{-1}, \quad (1)$$

where A stands for normalization, α represents the spectral index, and ν_b signifies the bending frequency.

We estimate the parameters of each PSD model (A and α for PL, and A , α , and ν_b for BPL) for the six sources using maximum likelihood (ML) and Markov chain Monte Carlo simulations (MCMC, Foreman-Mackey et al. 2013).

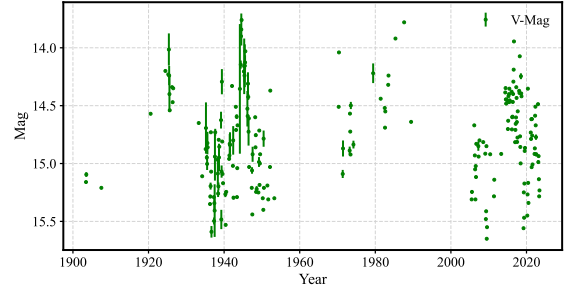
5. RESULTS AND DISCUSSIONS

We present the results of our GLSP and Wavelet analyses on the 6 candidate blazars in Table 2. In both types of periodicity analyses, we calculate the significance of each of the observed periods against red noise following both PL and BPL methods (Table 3 shows the PSD fit parameters). As initial selection criteria, we take 2σ as a threshold in at least two out of four reported significances. We also take the fraction of the time series inside the COI in the scalogram plot as a measure of the quality of detection; we set a limit of $\geq 30\%$ (see Appendix A2).

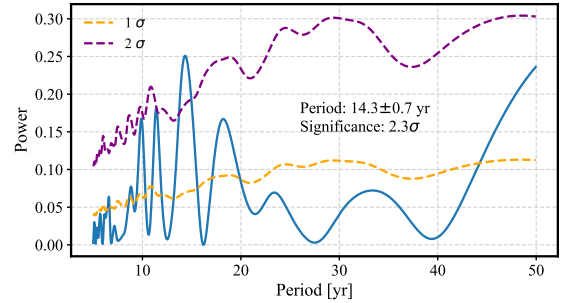
Following these selection criteria, the periods observed on the M 87 and MKN 180 LCs are considered nondetections. In the case of ~ 13 -yr period of MKN 180, none of the calculated significances are above two sigma (see Table 2). And for the observed period of ~ 45 -yr of M 87, $< 20\%$ of the LC timescale is within the COI (see Appendix A2). For the remaining 4 sources, we notice at least two $\geq 2\sigma$ significance, and the dominant period inside the COI spans at least 30% of the time-series length.

5.1. Candidates

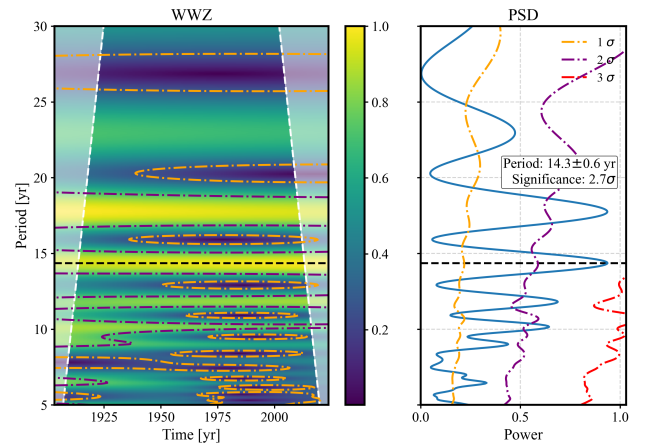
We consider the periods of the 4 sources (AP Librae, MKN 421, MKN 501, and PG 1246+586) as potential detections and further scrutinize the observed periodicity. We fit a sinusoidal signal on the LCs and take the goodness of fit (R^2) value as a relative measure of the quality of observed periods. As we do not expect the periodicity in blazar emission to follow a perfect sinusoid, we refrain from using these values as an absolute measure of the periodicity and rather compare the R^2 among the results. These values are reported in Table 2. Furthermore, we do a phase fold of the LCs with the observed periods, making visualization of a periodic signal easier, especially when the data is uneven and with gaps. Below, we discuss these additional studies in the periodicity for each blazar.



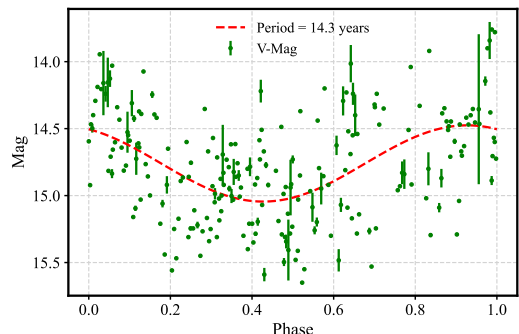
a) 28 days binned LC combined from DASCH and complementary databases.



b) GLSP periodogram with significance levels. The peak period of 14.3 ± 0.7 yr has a PL significance of 2.3σ .



c) WWZ scalogram and PSD showing the highest peak at 14.3 ± 0.6 yr with 2.7σ PL significance.



d) 14.3 yr phase-folded LC with a sinusoidal fit. The R^2 of the sine fit is 0.27.

Figure 2. AP Librae LC and periodicity analysis results.

Blazar name	GLSP (yr)	S/N	R ²	WWZ (yr)	S/N	R ²
AP Librae	14.3±0.7	PL: 2.3σ BPL: 2.3σ	0.270	14.3±0.6	PL: 2.7σ BPL: 3.0σ	0.271
M 87	45.4±1.1	PL: 0.8σ BPL: 0.7σ	0.26	49.0±7.0	PL: 2.3σ BPL: 2.7σ	0.29
MKN 180	13.6±2.2	PL: 1.1σ BPL: 1.1σ	0.03	12.1±0.8	PL: 1.5σ BPL: 1.6σ	0.06
MKN 421	47.6±9.5	PL: 2.3σ BPL: 2.4σ	0.23	54.2±8.8	PL: 2.7σ BPL: 2.8σ	0.23
MKN 501	57.7±8.5	PL: 1.5σ BPL: 1.5σ	0.35	53.8±13.5	PL: 2.1σ BPL: 2.2σ	0.37
PG 1246+586	36.4±5.2	PL: 2.0σ BPL: 2.2σ	0.09	31.7±3.1	PL: 1.2σ BPL: 1.8σ	0.15
	13.1±0.3	PL: 1.9σ BPL: 2.1σ	0.126	12.9±0.6	PL: 1.5σ BPL: 2.1σ	0.128

Table 2. GLSP and Wavelet analysis results, their significance, and R² values of sinusoidal fits.

Blazar	PL		BPL		
	A	α	A	ν _{bend}	α
AP Librae	0.0090±0.0020	0.89±0.09	0.12±0.01	0.130±0.020	3.45±0.32
M 87	0.0012±0.0001	0.91±0.04	0.11±0.02	0.030±0.010	1.13±0.08
MKN 180	0.0040±0.0020	0.71±0.05	0.06±0.01	0.100±0.060	1.26±0.23
MKN 421	0.0080±0.0010	0.74±0.03	0.29±0.07	0.020±0.010	1.02±0.08
MKN 501	0.0015±0.0002	1.12±0.23	0.44±0.02	0.012±0.003	1.31±0.03
PG 1246+586	0.0320±0.0020	0.89±0.08	0.38±0.02	0.020±0.010	0.85±0.05

Table 3. PL and BPL parameters for the sample blazars.

AP Librae—For the source AP Librae, we show the LC, periodicity analysis results, and the 14.3-yr phase-folded LC in Figure 2. We see similar R^2 values for GLSP and WWZ periods. When compared with other sources, the goodness of fit is also high. The reported significances are highest for AP Librae compared to other sources, and we do not notice any gaps on the phase-folded LC (see Figure 2).

MKN 421—For this source, we observe a ~ 55 yr period on the LC with $> 2\sigma$ significance with the same R^2 value of 0.23 for GLSP and WWZ periods. The observed period falls at the upper range of the search period, where the impact of red noise is more pronounced, and we notice only a limited fraction of the signal ($\sim 40\%$) inside the COI. The phase-folded LC, however, does not show data gaps.

MKN 501—We observe a ~ 55 yr period for MKN 501 with $> 2\sigma$ significance on only the wavelet analysis. The R^2 values are similar for GLSP and WWZ periods and are highest among the sources. However, we notice a limited signal ($\sim 40\%$) inside the COI, and the peak of this period is also not well defined in the wavelet PSD

plot (see Appendix A2). We also do not notice gaps in the phase-folded LC data for this source.

PG 1246+586—For this source, we observe two simultaneous periods of ~ 35 yr and ~ 13 yr. However, the R^2 values for the GLSP and WWZ periods are the lowest among our candidate sources, indicating the poorest periodic behavior among our sources of interest. The 36-yr phase-folded LC shows a contiguous gap in the signal (see Figure 3), suggesting that the data gap influences this period, but we do not notice such gaps on the 13 yr phase-folded LC.

5.2. Gap study for candidate sources

The gaps in the LCs could have an impact on the observed periods of AP Librae, MKN 421, MKN 501, and PG 1246+586. This fact demands further analysis of the impact of the gaps in the data. This section discusses the effect of the gaps in the significance estimation and the false periodicities due to the uneven sampling for each of our sources. For this analysis, we only report our candidates' GLSP period(s) and PL significance for simplicity.

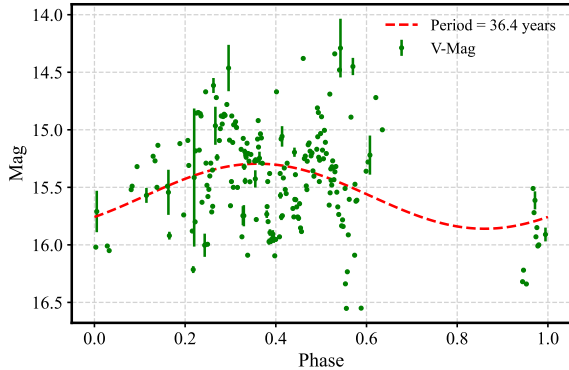


Figure 3. 36.4 yr phase-folded LC of PG 1246+586. The prominent gap in the phase-folded LC shows the gaps’ impact in the spurious detection of the period.

We conduct an analogous analysis to §3.1 using our sample blazar’s binned LCs. We use the PL fit parameters from Table 3 for each of the sources. We maintain the same sampling and observation uncertainties for each simulated signal as the original LC. For instance, for each AP Librae-like red-noise LC, we keep the same temporal sampling as the original binned LC and simulate the magnitudes with PL fit parameters $A = 0.009$ and $\alpha = 0.002$ and on top of that, we assign magnitude errors by resampling the errors from the original LC. The results of this analysis are presented in a period-significance distribution plot. Where the distribution shows the observed peak periods and significances in the periodogram of blazar-like red-noise LCs. The vertical red dotted lines represent enhancement locations, and the red + symbol indicates the observed GLSP period and PL significance from Table 2. We discuss the results in detail for each source below.

AP Librae—The period-significance distribution for AP Librae-like LCs reveals notable spikes in the period density plot around 10 and 30 yr (see the top panel of Figure 4), in contrast to the general gap study (see the top panel of Figure 1). Additionally, we observe an overall elevation in significance values for all detected periods, especially for periods < 30 yr (see the right panel of Figure 4). The period we observe (14.3 yr) lies within the enhancement. Additionally, the significance density plot is centered at 1.9σ ($> \sigma_{\text{mean}}$ from §3.1), suggesting the significance value we report (2.2σ) can be caused by the nature of the gaps.

MKN 421—The distribution for MKN 421-like LCs reveals notable spikes in the period density plot around 10 and 30 yr (see the top panel of Figure 5). Furthermore, we observe an overall elevation in significance values for all detected periods, similar as for AP Librae. The main

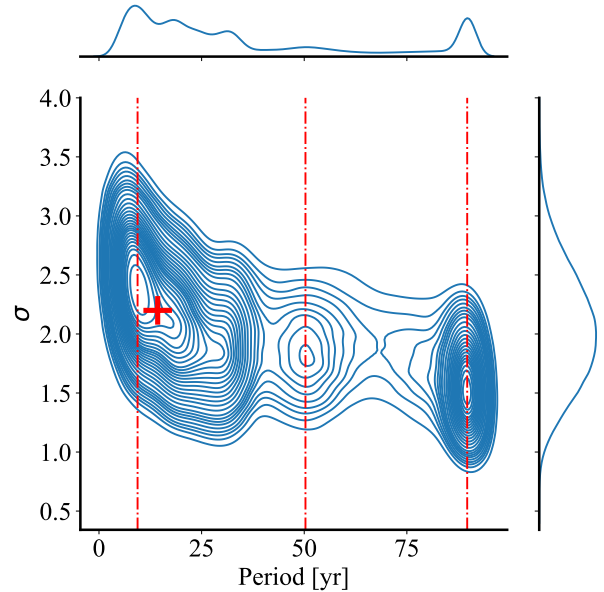


Figure 4. For AP Librae-like red-noise LCs, enhancements are at 9.4, 50.3, and 89.7 yr with the observed period (+) of 14.3 yr (2.2σ) inside the enhancement due to the gap.

plot shows that the observed period (47.6 yr) lies outside the enhancement region, and the significance density plot on the right is centered at 1.6σ ($> \sigma_{\text{mean}}$). Our result suggests the period and its significance value we report (2.2σ) is less likely due to the gaps.

MKN 501—For the MKN 501-like LCs, the period density function (top panel of Figure 6) shows a slight enhancement around 57 yr. Although this enhancement is relatively minor, the significance distribution (right panel) has a mean of 1.5σ , which puts our observed period’s significance of 1.5σ within the possibility of spurious detection. We conclude that this period could be due to the gaps in the observation.

PG 1246+586—For this source, the period density plot on the top panel of Figure 7 shows enhancements for periods less than 40 yr. Both the observed periods fall within this enhancement region. The significance density plot has a mean of 1.8σ , putting our observed periods and reported significance into question.

Given a multitude of quality issues with the observed periods, such as the unreliable significance values, the gap in phase-folded LC, and the low R^2 values of the fits of both periods, we omit PG 1246+586 from further analyses.

From the analysis of the sources of interest, only the ~ 50 -year period of MKN 421 is likely not an artifact of the gaps. More importantly, these findings corroborate the argument that gaps in time series data can yield spurious

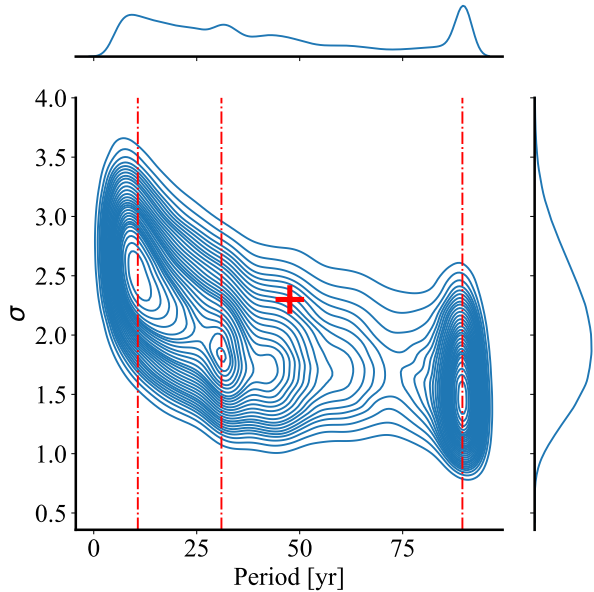


Figure 5. For MKN 421-like red-noise LCs, enhancements are at 10.7, 31.0, and 89.5 yr with the observed period (+) of 47.6 yr (2.3σ) away from the enhancement due to gap.

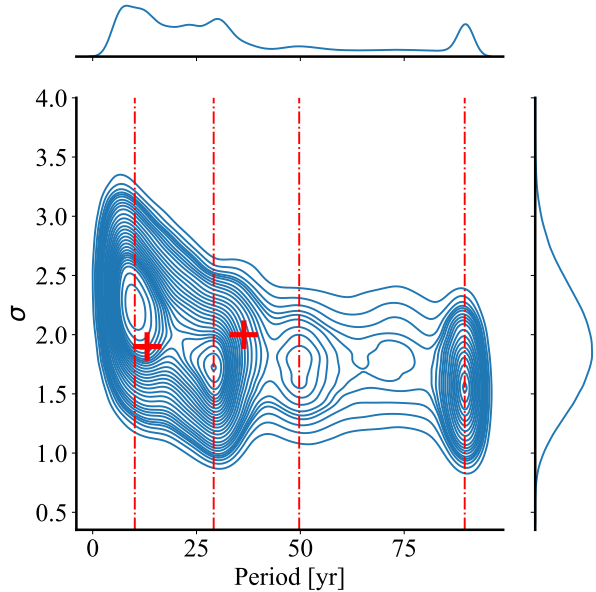


Figure 7. For PG 1246+586-like red-noise LCs, enhancements are at 10.1, 29.1, 49.7, and 89.6 yr with both observed periods (+) of 13.1 yr (1.9σ) and 36.4 yr (2.0σ) close to the enhancement due to the gap.

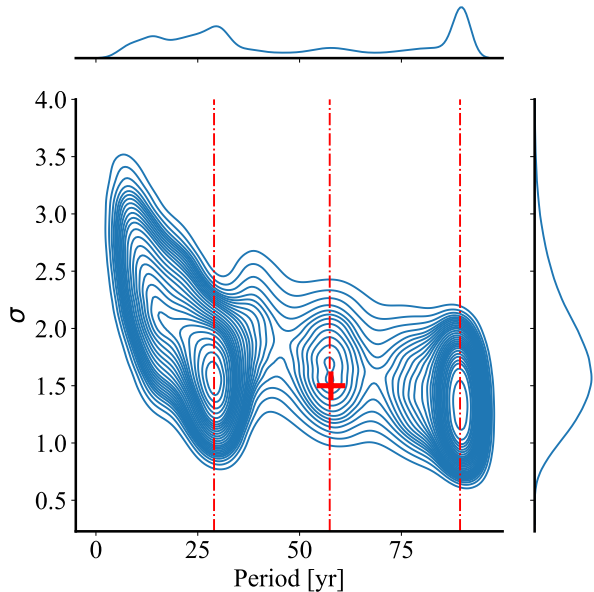


Figure 6. For MKN 501-like red-noise LCs, enhancements are at 29.0, 57.4, and 89.4 yr with the observed period (+) of 57.7 yr (1.5σ) inside the enhancement due to the gap.

periods with higher significance, suggesting caution in interpreting the observed period in the LCs.

5.3. Global significance

The significance obtained from our analysis methods needs adjustment to account for the look-elsewhere effect, as outlined by [Gross & Vitells \(2010\)](#). This correction yields the global significance of the detected period, which can be approximated using the formula:

$$p_{\text{global}} = 1 - (1 - p_{\text{local}})^N, \quad (2)$$

where N represents the trial factor. The expression calculates this trial factor:

$$N = P \times B, \quad (3)$$

where P denotes the number of independent periods (frequencies) in each periodogram, and B is the number of blazars in our sample. The value of P is estimated through Monte Carlo simulations, utilizing the algorithm described by [Peñil et al. \(2022\)](#) and employing 10^6 simulated light curves generated using the method by [Timmer & Koenig \(1995\)](#). Through an exploration of values of P , we aim to achieve the best fit to the experimental relationship of local-global significance, selecting a value of P to correct significance levels of $\geq 2\sigma$ obtained in our analysis. With a limit of $P \leq 100$ to balance computational efficiency and resolution, we find $P = 43$.

Given that we analyzed six blazars ($B = 6$), the number of independent periods determines the trial factor, resulting in a total trial factor of $N = 258$. Apply-

ing this factor to Equation 2, the global significance for a significance level of 2σ is approximately zero. This means the periods we observe in this work are statistically non-significant.

5.4. False alarm probability

FAP is the probability that a blazar-like, red-noise LC produces a peak period with a given local significance. We use 2σ as a representative value of the local significances, as discussed in § 5 for FAP calculation. We generate 10^6 LCs based on two PSD models: PL and BPL, employing the parameters estimated in § 4.3 while maintaining the same sampling interval as the 28 days binned LCs of our sources. We determine the following false detection rates for our sample blazars.

Our analysis reveals approximately 36.7% and 27.6% false detection rates for PL and BPL, respectively, for AP Librae, 24.4% and 16.1% for MKN 421, and 10.8% and 22.7% for MKN 501. These values correspond to a global significance of $\sim 0.3\sigma - 1.2\sigma$, which are again statistically non-significant.

5.5. Light curve reconstruction and prediction

Even though the periods observed in the LCs of AP Librae, MKN 421, and MKN 501 can not be conclusively attributed to genuine physical processes, we perform a sinusoidal fit on those blazar's LCs and predict the next high and low emissions. While the underlying periodic behavior (if genuine) may not strictly follow a sinusoidal curve, extending the fit and predicting the future emissions might provide insights into the underlying cyclic pattern. We present the sinusoidal fit and the predictions in Figures 8, 9, and 10.

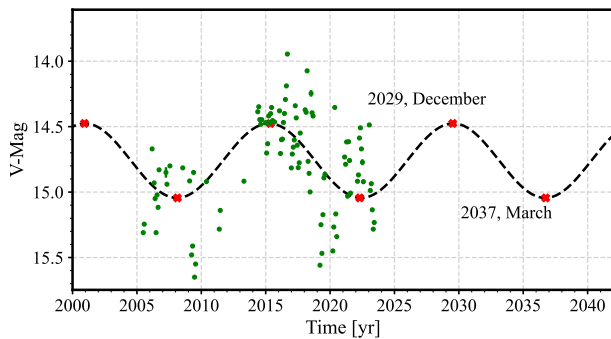


Figure 8. Prediction of the optical emission from the sinusoidal reconstruction of AP Librae. The next maxima and minima will occur in 2029, December and 2037, March, respectively.

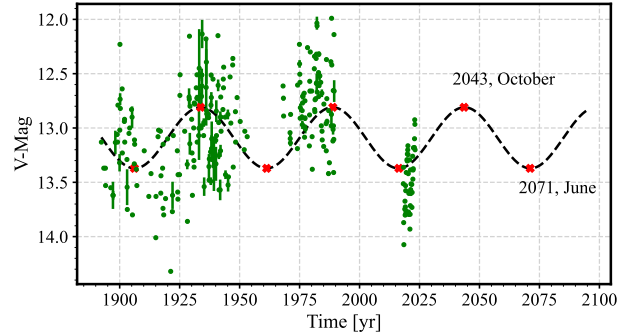


Figure 9. Prediction of the optical emission from the sinusoidal reconstruction of MKN 421. The next maxima and minima will occur in 2043, October and 2071, June, respectively.

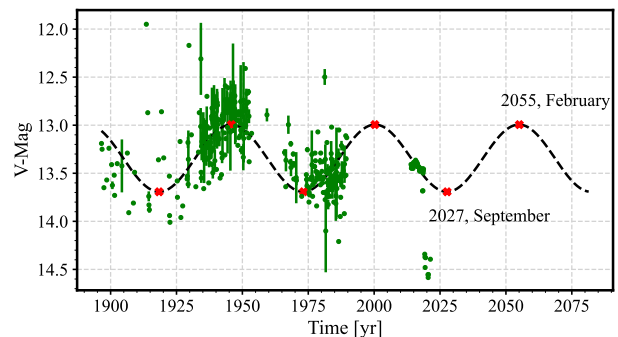


Figure 10. Prediction of the optical emission from the sinusoidal reconstruction of MKN 501. The next minima and maxima will occur in 2027, September and 2055, February, respectively.

We searched historical optical data for the blazars included in the 2FHL *Fermi*-LAT catalog. As a result, we found data for 11 blazars. We exclude PG 1553+113 from our study as it was studied in our previous work (see A24). And from the remaining 10 blazars, we excluded seven more (B2 0716+33, PKS 0736+01, PKS 0754+100, PKS 1424+240, PKS 1440-389, S5 1039+81, and TXS 1055+567) because their data did not meet our requirement in terms of percentage of gaps in their LCs. Out of the remaining six sources, we found hints of QPOs in four sources: AP Librae, MKN 421, MKN 501, and PG 1246+586. We found a QPO of 14.3 yr with a local significance of 2.2σ for AP Librae, 47.6 yr (2.3σ) for MKN 421, 57.7 yr (1.5σ) for MKN 501, and double periods of 13.1 yr (1.9σ) and 36.4 yr (2.0σ) for PG 1246+586.

All four of the QPOs we reported are not statistically significant after correcting for the look elsewhere effect. The global significances were $\sim 0\sigma$'s, and the FAPs were

6. SUMMARY AND CONCLUSIONS

$\sim 0.3\sigma - 1.2\sigma$. In addition to that, our gap-impact analysis on blazar-like red-noise signals showed that the observed periods of three sources (AP Librae, MKN 501, and PG 1246+586) are likely an artifact of the nature of data sampling, specifically the gaps in the observation.

We found that the MKN 421's ~ 50 yr period was likely not an artifact of the sampling or gaps. However, more observational data is needed to test this low-frequency QPO.

With more continuous monitoring of blazars in optical and other wavelengths, we could determine whether the low-significance QPOs we found are real. If genuine, this would allow us to constrain the properties of the central engine and test binary black hole hypotheses. Furthermore, decade-long periodicities could indirectly identify binary systems, potentially identifying merger events for future gravitational wave detectors.

7. ACKNOWLEDGMENTS

We want to thank all the observatories from which we used data. The DASCH project at Harvard is grateful for partial support from NSF grants AST-0407380, AST-0909073, and AST-1313370. Funding for APPLAUSE has been provided by DFG (German Research Foundation, Grant), Leibniz Institute for Astrophysics Potsdam (AIP), Dr. Remeis Sternwarte Bamberg (University Nuernberg/Erlangen), the Hamburger Sternwarte (University of Hamburg) and Tartu Observatory. Plate material also has been made available from Thüringer Landessternwarte Tautenburg, and from the archives of the Vatican Observatory. We thank the Las Cumbres Observatory and its staff for their continuing support of the ASAS-SN project. ASAS-SN is supported by the Gordon and Betty Moore Foun-

ation through grant GBMF5490 to the Ohio State University, and NSF grants AST-1515927 and AST-1908570. Development of ASAS-SN has been supported by NSF grant AST-0908816, the Mt. Cuba Astronomical Foundation, the Center for Cosmology and Astroparticle Physics at the Ohio State University, the Chinese Academy of Sciences South America Center for Astronomy (CAS-SACA), the Villum Foundation, and George Skestos. The AAVSO database: Kafka, S., 2021, Observations from the AAVSO International Database, <https://www.aavso.org>. The National Aeronautics and Space Administration funds the CSS survey under Grant No. NNG05GF22G issued through the Science Mission Directorate Near-Earth Objects Observations Program. The Catalina Real-Time Transient Survey is supported by the U.S. National Science Foundation under grants AST-0909182 and AST-1313422. Based on observations obtained with the Samuel Oschin Telescope 48-inch and the 60-inch Telescope at the Palomar Observatory as part of the Zwicky Transient Facility project. ZTF is supported by the National Science Foundation under Grant No. AST-2034437 and a collaboration including Caltech, IPAC, the Weizmann Institute for Science, The Oskar Klein Center at Stockholm University, the University of Maryland, Deutsches Elektronen-Synchrotron and Humboldt University, the TANGO Consortium of Taiwan, the University of Wisconsin at Milwaukee, Trinity College Dublin, Lawrence Livermore National Laboratories, and IN2P3, France. Operations are conducted by COO, IPAC, and UW.

S.A. and P.P. acknowledge funding from NASA under contracts 80NSSC24K0635, 80NSSC23K1040, 80NSSC23K0294 and 80NSSC22K1578.

A.D. is thankful for the support received from the Proyecto PID2021-126536OA-I00, funded by MCIN/AEI/10.13039/501100011033.

REFERENCES

- Abdo, A., Ackermann, M., Ajello, M., et al. 2009, *The Astrophysical Journal*, 708, 1310
- Acciari, V., Aliu, E., Arlen, T., et al. 2011, *The Astrophysical Journal*, 738, 25
- Ackermann, M., Ajello, M., Atwood, W. B., et al. 2016, *The Astrophysical Journal Supplement Series*, 222, 5
- Adhikari, S., Peñil, P., Westernacher-Schneider, J. R., et al. 2024, *The Astrophysical Journal*, 965, 124, doi: [10.3847/1538-4357/ad310a](https://doi.org/10.3847/1538-4357/ad310a)
- Arbet-Engels, A., Baack, D., Balbo, M., et al. 2021, *Astronomy & Astrophysics*, 647, A88
- Astropy Collaboration, Price-Whelan, A. M., Lim, P. L., et al. 2022, *ApJ*, 935, 167, doi: [10.3847/1538-4357/ac7c74](https://doi.org/10.3847/1538-4357/ac7c74)
- Bhatta, G. 2021, *The Astrophysical Journal*, 923, 7
- Chakraborty, N., Cologna, G., Kastendieck, M. A., et al. 2015, arXiv preprint arXiv:1509.04893
- Chakraborty, N., & Rieger, F. M. 2020, arXiv e-prints, arXiv:2010.01038, doi: [10.48550/arXiv.2010.01038](https://doi.org/10.48550/arXiv.2010.01038)
- Dey, L., Valtonen, M. J., Gopakumar, A., et al. 2018, *ApJ*, 866, 11, doi: [10.3847/1538-4357/aadd95](https://doi.org/10.3847/1538-4357/aadd95)
- Drake, A. J., Djorgovski, S. G., Mahabal, A., et al. 2009, *ApJ*, 696, 870, doi: [10.1088/0004-637X/696/1/870](https://doi.org/10.1088/0004-637X/696/1/870)
- Emmanoulopoulos, D., McHardy, I. M., & Papadakis, I. E. 2013, *MNRAS*, 433, 907, doi: [10.1093/mnras/stt764](https://doi.org/10.1093/mnras/stt764)

- Filippenko, A. V., Li, W., Treffers, R., & Modjaz, M. 2001, in *International Astronomical Union Colloquium*, Vol. 183, Cambridge University Press, 121–130
- Foreman-Mackey, D., Hogg, D. W., Lang, D., & Goodman, J. 2013, *PASP*, 125, 306, doi: [10.1086/670067](https://doi.org/10.1086/670067)
- Foster, G. 1996, *The Astronomical Journal*, 112, 1709
- Grindlay, J., Tang, S., Simcoe, R., et al. 2009, in *Astronomical Society of the Pacific Conference Series*, Vol. 410, *Preserving Astronomy's Photographic Legacy: Current State and the Future of North American Astronomical Plates*, ed. W. Osborn & L. Robbins, 101. <https://ui.adsabs.harvard.edu/abs/2009ASPC..410..101G>
- Gross, E., & Vitells, O. 2010, *European Physical Journal C*, 70, 525, doi: [10.1140/epjc/s10052-010-1470-8](https://doi.org/10.1140/epjc/s10052-010-1470-8)
- Gupta, A. C., Kushwaha, P., Carrasco, L., et al. 2022, *The Astrophysical Journal Supplement Series*, 260, 39
- Jurkevich, I., Usher, P., & Shen, B. 1971, *Astrophysics and Space Science*, 10, 402
- Khider, D., Athreya, P., Ratnakar, V., et al. 2020, in *Proceedings of the Sixth Workshop on Mining and Learning from Time Series (MiLeTS)*, held in conjunction with the 26th ACM SIGKDD Conference on Knowledge Discovery and Data Mining (KDD'20)
- Kochanek, C. S., Shappee, B. J., Stanek, K. Z., et al. 2017, *PASP*, 129, 104502, doi: [10.1088/1538-3873/aa80d9](https://doi.org/10.1088/1538-3873/aa80d9)
- Masci, F. J., Laher, R. R., Rusholme, B., et al. 2019, *PASP*, 131, 018003, doi: [10.1088/1538-3873/aae8ac](https://doi.org/10.1088/1538-3873/aae8ac)
- Papadakis, I., & Lawrence, A. 1993, *Monthly Notices of the Royal Astronomical Society*, 261, 612
- Peñil, P., Ajello, M., Buson, S., et al. 2022, arXiv e-prints, arXiv:2211.01894, doi: <https://doi.org/10.48550/arXiv.2211.01894>
- Peñil, P., Domínguez, A., Buson, S., et al. 2020, *The Astrophysical Journal*, 896, 134
- Peñil, P., Westernacher-Schneider, J., Ajello, M., et al. 2024, *Monthly Notices of the Royal Astronomical Society*, 527, 10168
- Peterson, B. M. 1997, *An introduction to active galactic nuclei* (Cambridge University Press)
- Qian, S., Britzen, S., Krichbaum, T., & Witzel, A. 2019, *Astronomy & Astrophysics*, 621, A11
- Qian, S., Britzen, S., Witzel, A., Krichbaum, T., & Kun, E. 2018, *Astronomy & Astrophysics*, 615, A123
- Rieger, F. M. 2004, *The Astrophysical Journal*, 615, L5
- . 2019, *Galaxies*, 7, doi: [10.3390/galaxies7010028](https://doi.org/10.3390/galaxies7010028)
- Shappee, B. J., Prieto, J. L., Grupe, D., et al. 2014, *ApJ*, 788, 48, doi: [10.1088/0004-637X/788/1/48](https://doi.org/10.1088/0004-637X/788/1/48)
- Tavani, M., Cavaliere, A., Munar-Adrover, P., & Argan, A. 2018, *The Astrophysical Journal*, 854, 11
- Timmer, J., & Koenig, M. 1995, *A&A*, 300, 707. <https://adsabs.harvard.edu/full/1995A%26A...300..707T/0000710.000.html>
- Tukey, J. W., et al. 1977, *Exploratory data analysis*, Vol. 2 (Reading, MA)
- Tuvikene, T., Edelmann, H., Groote, D., & Enke, H. 2014, *Astroplate 2014*, 127
- Urry, C. M., & Padovani, P. 1995, *Publications of the Astronomical Society of the Pacific*, 107, 803
- VanderPlas, J. T. 2018, *The Astrophysical Journal Supplement Series*, 236, 16, doi: [10.3847/1538-4365/aab766](https://doi.org/10.3847/1538-4365/aab766)
- Vaughan, S., Edelson, R., Warwick, R., & Uttley, P. 2003, *Monthly Notices of the Royal Astronomical Society*, 345, 1271
- Wagner, S., & Witzel, A. 1995, *Annual Review of Astronomy and Astrophysics*, 33, 163
- Wiita, P. J. 2006, arXiv e-prints, astro, doi: [10.48550/arXiv.astro-ph/0603728](https://doi.org/10.48550/arXiv.astro-ph/0603728)
- Zhu, S., & Xue, Y. 2016, *The Astrophysical Journal*, 825, 56

APPENDIX

This section reports the LCs of the blazars with historical data and the results of the WWZ for those selected according to the gap criterion defined in §3.2.

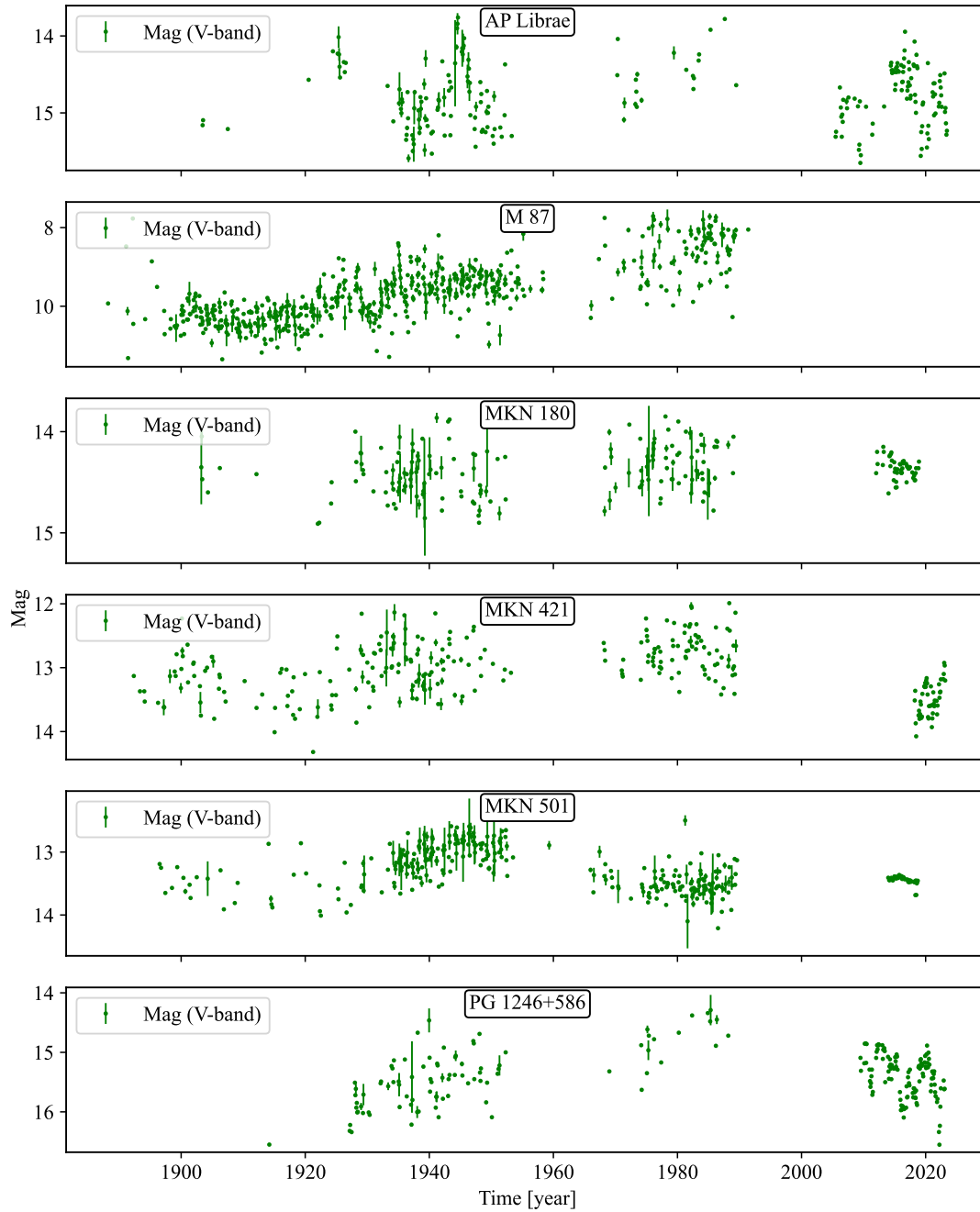


Figure A1. 28 days binned light curves of blazars selected for periodicity study.

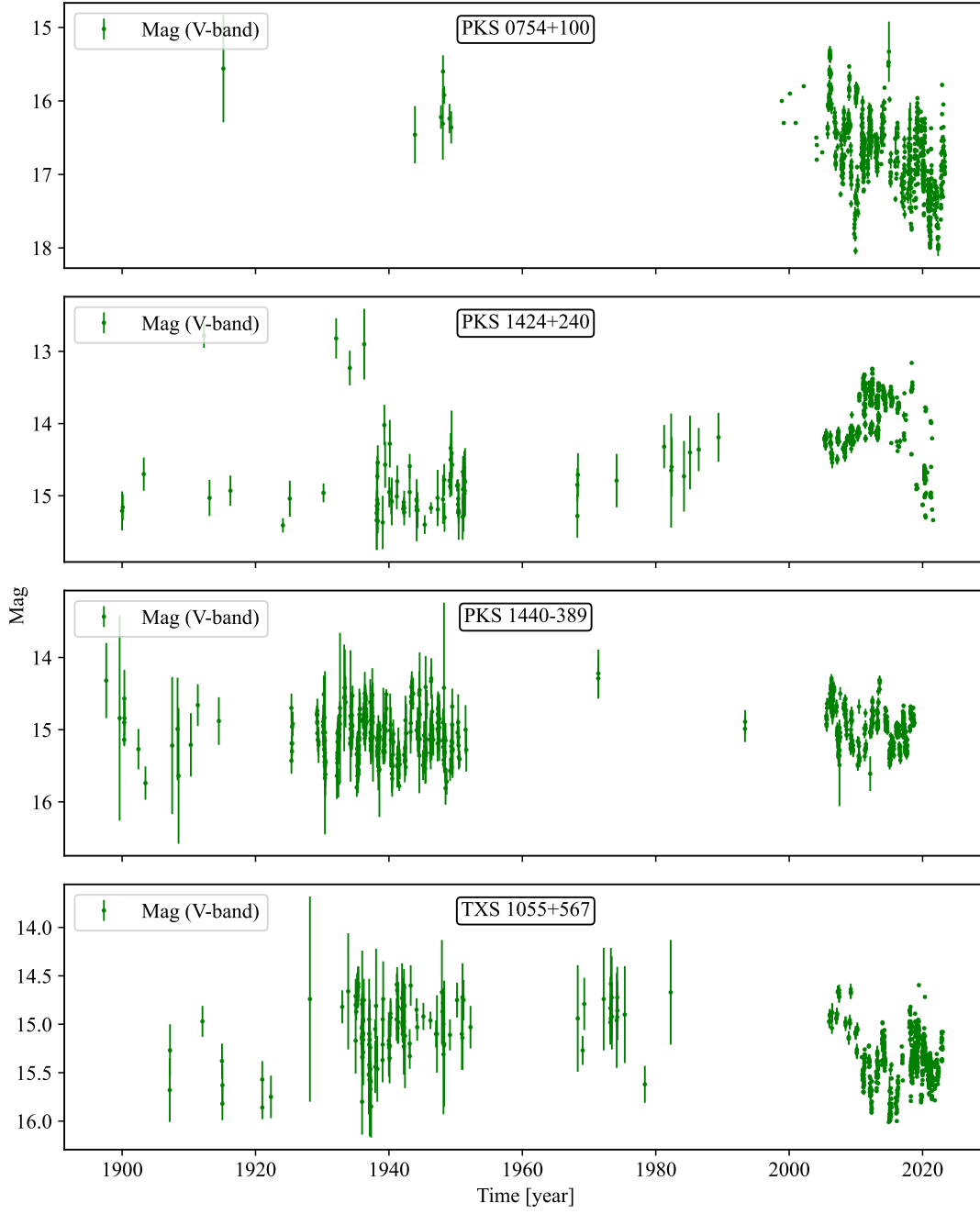


Figure A1. (Continued).

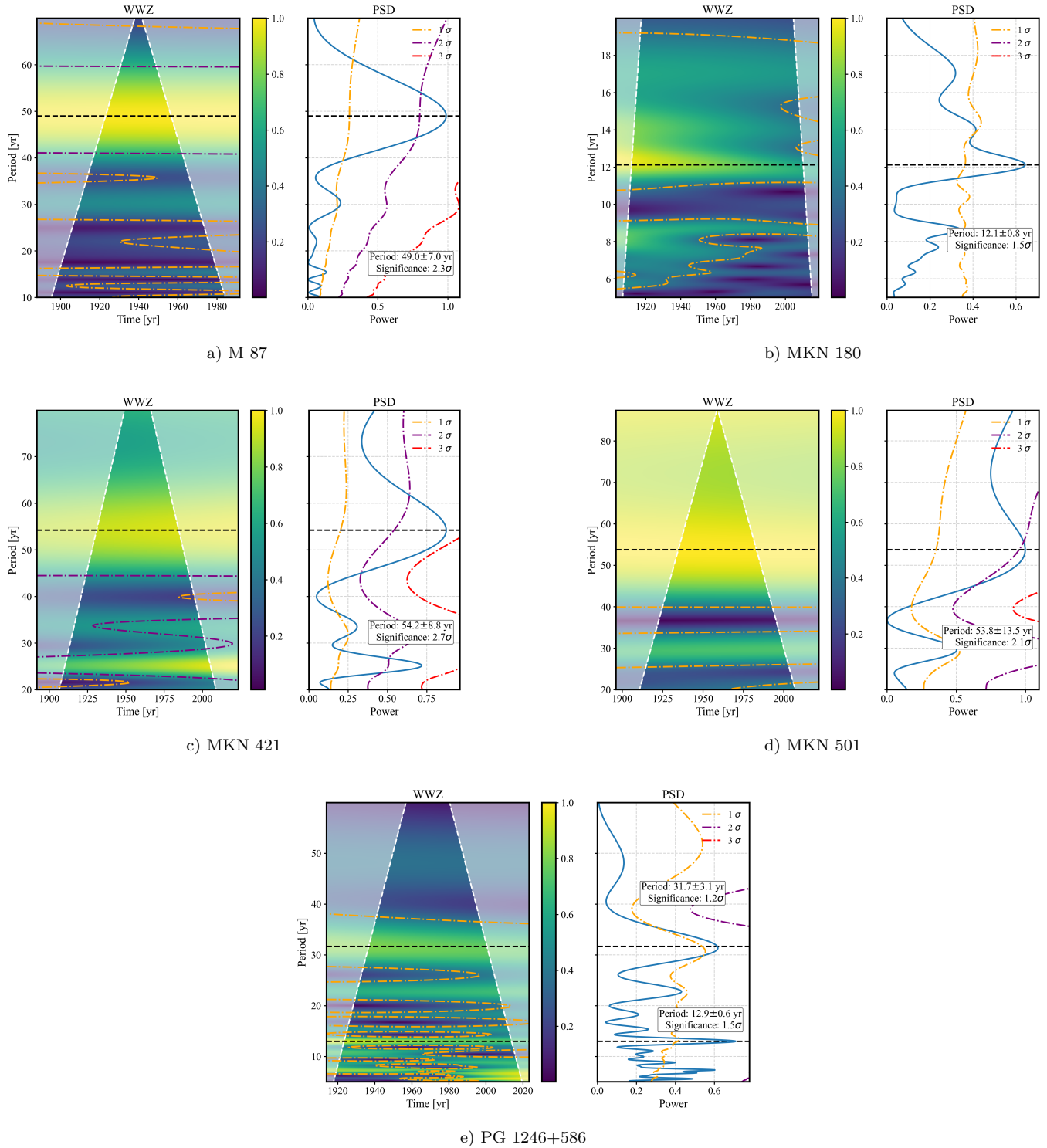


Figure A2. WWZ scalograms and PSD plot for the rest of the sources from Table 2. The shaded white region shows the region outside the COI, the dashed black lines represent prominent peaks, and dash-dot lines of different colors represent different significance and contour levels.